Progress In Electromagnetics Research, PIER 9, 265–288, 1994

THEORETICAL STUDY OF RADIATION PROPERTIES OF A FINITE-LENGTH THIN-WIRE CHIROSTRIP ANTENNA USING DYADIC GREEN'S FUNCTIONS AND METHOD OF MOMENTS

P. Pelet and N. Engheta

1. Introduction

Chirality in electromagnetics, chiral materials, and their potential applications have been the subject of extensive research in electromagnetics, optics, and microwave communities in recent years [1–30]. It is known that chiral materials, when isotropic, support two characteristic wavenumbers $k_{\pm}$ independent of the direction of propagation. These wavenumbers, which can be explicitly written in terms of the material parameters as $k_{\pm} = \pm\omega\mu_c\xi_c + \omega\sqrt{\mu_c\varepsilon_c + \mu_c^2\xi_c^2}$, correspond to right– and left–circularly polarized eigenmodes of propagation [6]. Therefore, isotropic chiral materials are circular polarization birefringent. In the past several years, there has been increasing interest in the study of chiral materials and their potential applications in optical, microwave

and millimeter–wave frequencies [1–30]. One such potential application is the suggestion of using chiral slabs as possible substrates and superstrates for printed–circuit devices, such as microstrip antennas [17–30]. This combination was named chirostrip antennas [17]. Several canonical theoretical problems involving chiral materials and microstrip antennas have been studied and reported in the literature [17–30]. In this paper, we discuss the radiation properties of a center–fed finite–length thin–wire chirostrip antenna over a thick grounded lossless chiral slab. This antenna can be conceptually thought of as a thin cylindrical wire over the surface of a grounded lossless chiral slab. Pozar has provided an excellent analysis for a single square patch antenna and for an infinite array of square microstrip antennas over grounded chiral slab [24]. Bhattacharyya and Lakhtakia have also studied the rectangular microstrip patch antenna over chiral substrates using Baltrami field formulation [25]. Kluskens and Newman have reported their thorough study of surface current distributions and dispersion characteristics of guided waves along an infinite microstrip transmission line over grounded chiral slabs [19]. Jaggard et. al [15] and Bhattacharyya et. al [16] have studied current distributions along finite–length antennas, but in an unbounded chiral media. Yin and Wang [26–28] and Ren [29] have done a series of studies on radiation characteristics such as Green's functions and canonical antennas in chiral layers. Toscano and Vegni have studied spectral dyadic Green's functions for grounded chiral slabs [18]. In our previous work, we have studied the case of two–dimensional chirostrip line antennas [20,21,23] and the case of a chirostrip infinitesimally short horizontal dipole [22,23]. For the chirostrip horizontal short dipole over thick substrates, we demonstrated theoretically that the handedness of the chiral substrate manifests itself in the radiation pattern of the dipole antenna, by causing the radiation pattern of the antenna to rotate around the axis normal to the substrate by an angle, which over some range of ξ_c, depends on the value of chirality. Although these canonical cases, i.e., infinitesimal dipole chirostrip and infinitely long line chirostrip antennas, may be adequate to approximately model problems involving very short or very long antennas on grounded chiral substrates, the methods developed for those problems need to be extended in order to take into account the finite length of a moderate–size thin–wire antenna lying on top of such substrates. Furthermore, in the previous analyses [18, 20–23, 26–29], given current distributions on the antenna were assumed

as is done for an infinitesimal dipole and two–dimensional infinitely long thin–wire antennas. However, for a center–fed finite–length thin–wire antenna over grounded chiral slabs, the current is neither known *a priori*, nor is uniform along the length of antenna. The knowledge of current distribution along a finite–length thin–wire chirostrip antenna will also enable us to analyze other electromagnetic properties of this antenna, such as radiation patterns and radiated power, etc.. Here, using dyadic Green's functions for a grounded chiral slab and the standard method of moments, we determine the current distribution along such chirostrip antennas for a thick chiral substrate. We then obtain the input impedance, radiation patterns, bandwidth, and some other radiation properties of this center–fed finite–length thin cylindrical wire chirostrip antenna.

2. Current Distribution Along a Center-Fed Finite-Length Thin-Wire Chirostrip Antenna (over a Thick Grounded Chiral Slab)

Let us consider a finite–length thin–wire chirostrip antenna shown in Fig. 1. This antenna consists of a very thin cylindrical wire printed on the surface of a thick grounded chiral slab of thickness d, permittivity ε_c, permeability μ_c, and chirality admittance ξ_c. The above region is free space with parameters ε_0 and μ_0. The antenna, which has the length L and the diameter $2a$, is driven at the center by a monochromatic voltage source $V_s = V_0 \exp(-i\omega t)$ where V_0 is a constant set to one volt in all our computations. The electric field $\mathbf{E}$ generated by this chirostrip antenna can then be expressed by $\mathbf{E} = i\omega\mu_c \int \overline{\overline{\Gamma}}_c(\mathbf{r}, \mathbf{r}') \cdot \mathbf{J}(\mathbf{r}')\, dV$ where $\overline{\overline{\Gamma}}_c(\mathbf{r}, \mathbf{r}')$ is the dyadic Green's function for the grounded chiral slab, and the integration is carried out over the unknown current $\mathbf{J}(\mathbf{r}')$ along the antenna. The vectors $\mathbf{r}'$ and $\mathbf{r}$ correspond to the source point and observation point, respectively, and can be written in cylindrical coordinates as $\mathbf{r}' = \rho'\mathbf{e}_{\rho'} + z'\mathbf{e}_{z'}$ and $\mathbf{r} = \rho\mathbf{e}_\rho + z\mathbf{e}_z$ where $\mathbf{e}_{\rho'}$, $\mathbf{e}_\rho$, $\mathbf{e}_{z'}$, and $\mathbf{e}_z$ are the usual unit vectors. The problem of dyadic Green's functions for a chiral slab and chiral layers has been studied extensively using a variety of techniques [18,19,22–30]. In our analysis here, we use the dyadic Green's function which is expressed in terms of cylindrical vector wave functions [See e.g., 23]. In the Appendix, for the sake of easy reference, the expres-

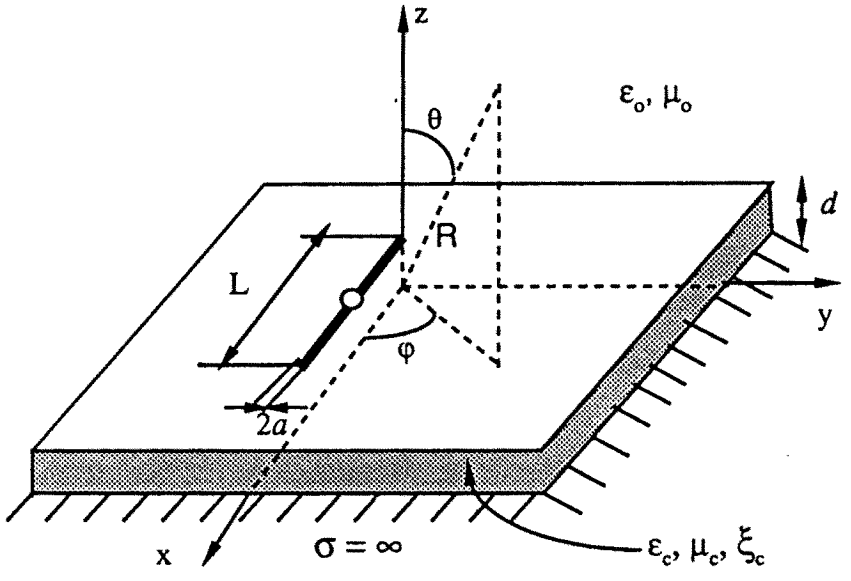

Figure 1. Center–fed finite–length thin–wire chirostrip antenna which can be thought of as a thin cylindrical wire of length L and radius a placed at the surface of a grounded chiral dielectric slab of thickness d. The material parameters of the slab are ε_c, μ_c, and ξ_c. The antenna is assumed to be fed at its center by a monochromatic voltage source. The Cartesian and spherical coordinate systems are also shown. The plane $z = 0$ is at the ground plane, and the antenna is extended from $x = 0$ to $x = L$.

sions of these dyadic Green's functions are given with no derivation. For detailed derivation of these Green's functions, the reader is referred to all related bibliographies given in the References, e.g., [23]. Here, the problem is to solve for the current distribution $\mathbf{J}(\mathbf{r}')$ by applying the boundary condition for the electric field at the antenna surface, i.e., by making the tangential electric field vanish at the surface of the antenna. [1] Here, we also assume that $a \ll \lambda_0$ where λ_0 is

[1] The boundary conditions at the surface of the chiral slab and at the ground plane are already satisfied by using the proper dyadic Green's functions $\underline{\underline{\Gamma}}_c(\mathbf{r}, \mathbf{r}')$.

the free–space wavelength. Therefore, the thin–wire approximation for the antenna can be used and the current distribution $\mathbf{J}(\mathbf{r}')$ can have the form $\mathbf{J}(\mathbf{r}') = I(x')\,\delta(y')\delta(z'-d)\mathbf{e_x}$ along the wire antenna, where $\mathbf{e_x}$ is a unit vector along the x–axis, and $\delta(.)$ is a Dirac delta function. The current $I(x')$ must satisfy the condition $I(0) = I(L) = 0$. To determine $I(x')$ completely, we use the standard method of moments and divide the wire antenna into N equal segments $\Delta = L/N$ [31]. Then the current distribution $I(x')$ is expanded in terms of an appropriate current basis $[\Phi_p(x')]_p$ with unknown coefficients $I_p s$ as $I(x') = \sum_{p=0}^{N-1} I_p \Phi_p(x')$. Many choices of basis functions $\Phi_p(x')$ are possible. Here we choose the sinusoidal basis functions. These basis functions are expressed as

$$I(x') = \begin{cases} I_p \dfrac{\sin\left[k_0\left(\Delta - |x' - x_p|\right)\right]}{\sin\left[k_0\Delta\right]} & \text{if } |x' - x_p| \le \Delta \\ 0 & \text{otherwise.} \end{cases} \tag{1}$$

where $k_0 = \omega\sqrt{\mu_0\varepsilon_0}$. The current distribution can then be obtained using the standard method of moments and the dyadic Green's functions for the grounded chiral slab. [2] Numerical results for the current distribution $I(x')$ are presented in Fig. 2 for different values of the slab's chirality admittance ξ_c. In Fig. 2, the real and imaginary parts of the current are plotted while the thickness d of the slab is kept constant at $d = 0.24\lambda_0$. [3] In all our computations, the radius a of the antenna is taken to be $0.0001\lambda_0$. As can be noted in this case, adding chirality increases the magnitude of the current, but does not change significantly the effective electrical length of the antenna. Once the current $I(x')$ is known, the input impedance can be determined by evaluating V_0/I_{in}, where I_{in} is the current at the feed location.

[2] The detailed description of steps taken in finding the current distribution here using the dyadic Green's function for this slab has not been given here, for the sake of brevity. Interested readers are referred to [23].

[3] We realize that the thickness of the slab should usually be much smaller than the free–space wavelength. Here, however, we have chosen $d = 0.24\lambda_0$, just as a numerical example for a parametric study to consider the effects such as surface waves in (thick) slabs. Clearly, the present numerical analysis can be applied for much thinner slabs.

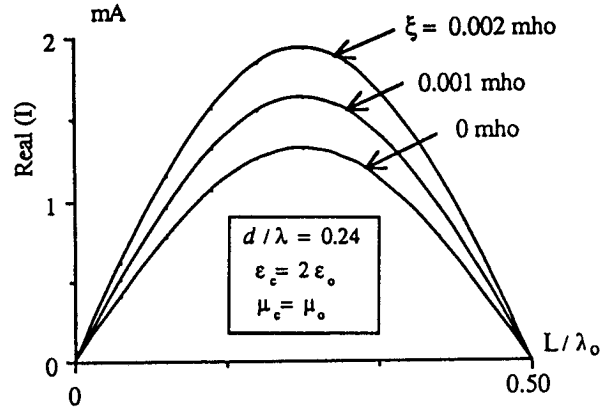

(A)

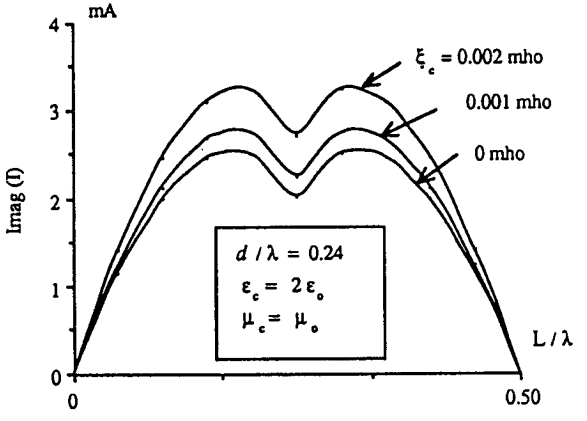

(B)

Figure 2. Real and imaginary parts of the current distribution along the chirostrip antenna shown in Fig. 1. The length $L = 0.50\lambda_0$ and radius $a = 0.0001\lambda_0$. The thickness of the thick slab is $d = 0.24\lambda_0$, permittivity $\varepsilon_c = 2\varepsilon_0$, permeability $\mu_c = \mu_0$. The cases $\xi_c = 0$, 0.001 and 0.002 mho are presented. We realize that the thickness of slab should usually be much smaller than the free–space wavelength. Here, however, we have chosen $d = 0.24\lambda_0$, just as a numerical example for a parametric study to consider the effects such as surface waves in (thick) slabs. Clearly, the present numerical analysis can be applied for much thinner slabs.

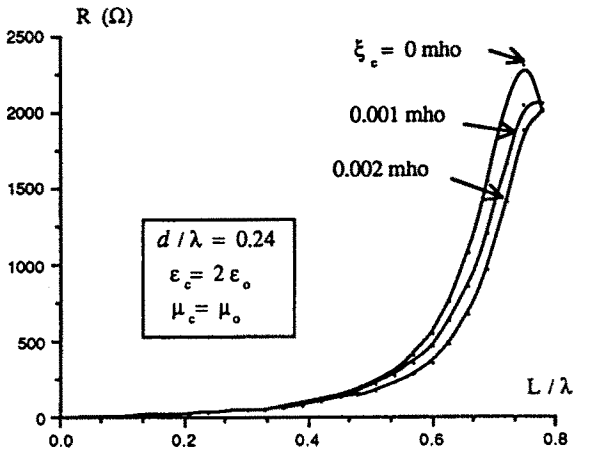

(A)

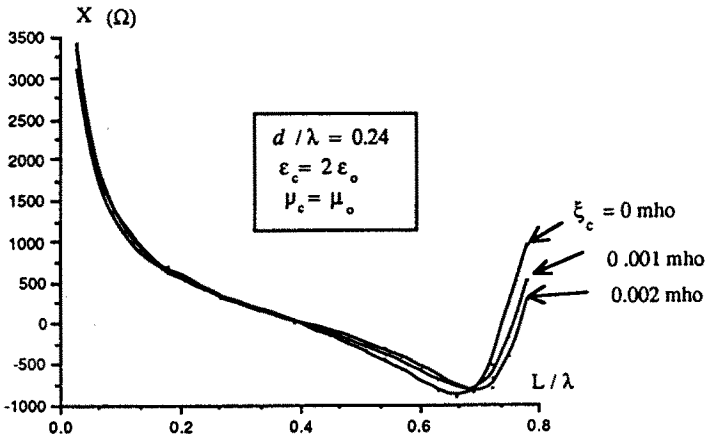

(B)

Figure 3. Real part R and imaginary part X of the input impedance of the chirostrip antenna of Fig. 1 as a function of the length L. The thickness of the thick slab is $d = 0.24\lambda_0$, the radius of the antenna is $a = 0.0001\lambda_0$, permittivity $\varepsilon_c = 2\varepsilon_0$, the permeability $\mu_c = \mu_0$, and $\xi_c = 0,\ 0.001$ and **0.002 mho.**

Numerical results for the input impedance $Z = R + \mathrm{i}X$ are given in Fig. 3 for several values of the chirality admittance ξ_c. The thickness d of the slab is kept at $0.24\lambda_o$ and the radius a is set to be $0.0001\lambda_o$. Since the voltage V_o is kept constant in all computations and, as can be seen from Fig. 2, the current magnitude can be increased, the total input power increases and thus R decreases. The resonant length L of this thin–wire antenna is, by definition, the length for which the imaginary part X of the input impedance vanishes. The evaluation of this resonant length L_r is therefore of interest since the bandwidth of the antenna can be defined by $BW = \frac{1}{L_r}\frac{2R_{\mathrm{res}}}{\frac{\partial X}{\partial(L/\lambda_o)}}$ where R_{res} is the value of the resonant input resistance and X the input reactance [32]. Figure 4 presents the resonant length L_r and the bandwidth BW as functions of the normalized slab thickness d/λ_o for several values of chirality ξ_c. One can notice the change in bandwidth when chirality is introduced in the slab. For instance, for $d/\lambda_o = 0.20$, the bandwidth is increased by 5 % when chirality is varied from 0 mho to 0.0015 mho.

3. Radiation Patterns of Finite-Length Thin-Wire Chirostrip Antenna

The knowledge of the current distribution allows us to determine the radiation pattern of the antenna for different values of chirality admittance ξ_c. Using the standard asymptotic expansions and the saddle–point technique, the following approximate closed form expression for the far–zone radiated fields can be obtained

$$\begin{Bmatrix} E_\theta \\ E\varphi \end{Bmatrix} = -\frac{\omega\mu_c \mathrm{e}^{\mathrm{i}(k_o R - \pi/4 + k_o d\cos\theta)}}{8\pi R} \begin{Bmatrix} F(\theta,\varphi) \\ G(\theta,\varphi) \end{Bmatrix} \sum_{p=1}^{N-1} \frac{I_p}{\sin(k_o\Delta)} \int_L \sin\left[k_o\left(\Delta - |x' - x_p|\right)\right] \mathrm{e}^{-\mathrm{i}k_o x' \sin\theta\cos\varphi}\, dx' \tag{2}$$

with

$$F(\theta,\varphi) = \left\{ \left(a^w - a^v + b^v - b^w + 2\mathrm{e}^{-2\mathrm{i}k_o d\cos\theta}\right)\cos\theta\cos\varphi + \mathrm{i}\left(a^v - a^w + b^v - b^w\right)\sin\varphi \right\}$$

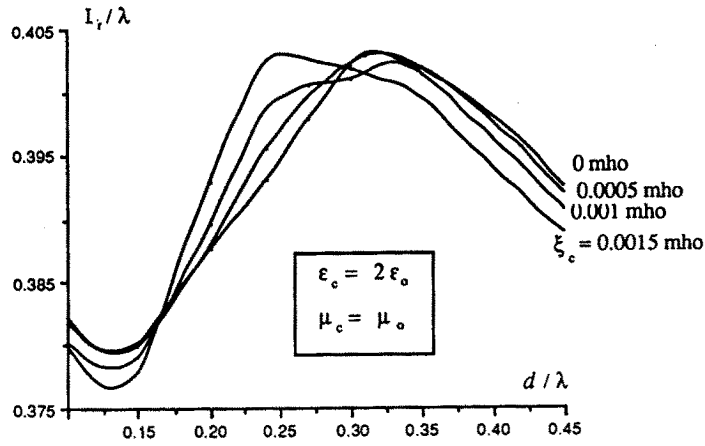

(A)

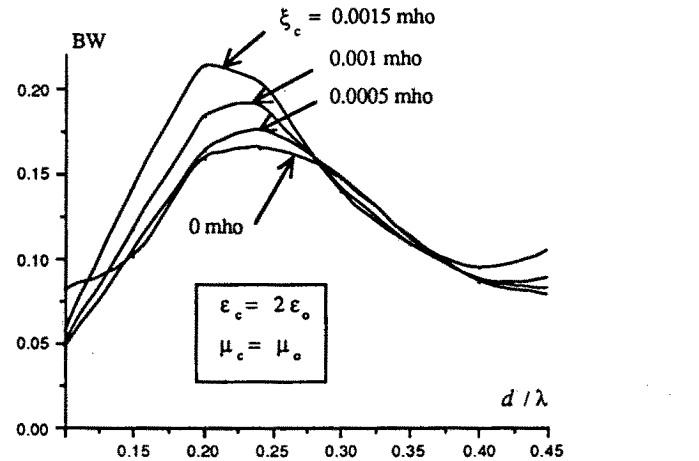

(B)

Figure 4. Resonant length L_r (shown in (A)) and bandwidth BW (shown in (B)) of the chirostrip antenna of Fig. 1 as a function of the normalized slab thickness d/λ_0 for values of the chirality admittance ξ_c = 0, 0.0005, 0.001, and **0.0015** mho. The radius of the antenna is $a = 0.0001\lambda_0$.

$$G(\theta,\varphi) = -\Big\{\Big(a^v + a^w + b^v + b^w + 2e^{-2ik_0 d\cos\theta}\Big)\sin\varphi + i\,(a^v + a^w - b^v - b^w)\cos\theta\cos\varphi\Big\}$$

where (R,θ,φ) are the usual spherical coordinates (shown in Fig. 1) and the other quantities have been defined in the Appendix. We note that $F(\theta,\varphi)$ and $G(\theta,\varphi)$ are very similar to the equivalent relations obtained for the horizontal infinitesimal dipole case [22,23]. Therefore, similar rotational characteristics for the radiation pattern can be expected here for this finite-length antenna over thick substrates. For the resonant case at $d/\lambda_0 = 0.30$, we obtain the plot of the radiation pattern and the pattern shift at a given elevation angle θ for several values of ξ_c. Figure 5 illustrates the radiation pattern of a resonant finite-length chirostrip antenna of the slab thickness $d/\lambda_0 = 0.30$, as a function of the azimuthal angle φ, for a fixed value of the elevation angle $\theta = 45°$, and for various chirality ξ_c. These results resemble to that of the chirostrip horizontal infinitesimally short dipole [22,23]. It is also worth noting that from (2) and expressions $F(\theta,\varphi)$ and $G(\theta,\varphi)$, one can evaluate the cross-polarization level in the E-plane and/or H-plane for such an antenna. Clearly for this antenna, cross-polarization can be developed due to chirality of the substrate, as is evident from $F(\theta,\varphi)$ and $G(\theta,\varphi)$ for $\varphi = 0°$, $180°$, and for $\varphi = 90°$, $270°$. This property might not be of interest in some antenna applications. However, the rotational characteristics of radiation patterns for such antennas might turn out to be an interesting feature. The physical insights and justifications of this rotational feature are given in [22,23]. The total radiated power P_{rad} can be obtained from $P_{\text{rad}} = \frac{1}{2\eta_0}\iint\left(|E_\theta|^2 + |E_\varphi|^2\right)dS \equiv \frac{1}{2}R_{\text{rad}}|I_{\text{in}}|^2$ where $\eta_0 = \sqrt{\mu_0/\varepsilon_0}$ and the integration is over the surface of the upper hemisphere with its radius approaching infinity. Here R_{rad} is used as the radiation resistance and I_{in} the input current. The radiation efficiency $\in$ of the antenna is then given as $\in = \dfrac{R_{\text{rad}}}{R_{\text{rad}} + R_{\text{surf}}}$ where R_{surf} is the contribution of the surface-wave power to the total radiation resistance $R = R_{\text{rad}} + R_{\text{surf}}$. In Fig. 6 and 7, the plots of R_{rad} of the radiated fields, R_{surf} of the surface-wave power, R_{res} the total radiation resistance at resonance, and $\in$ the radiation efficiency of this antenna

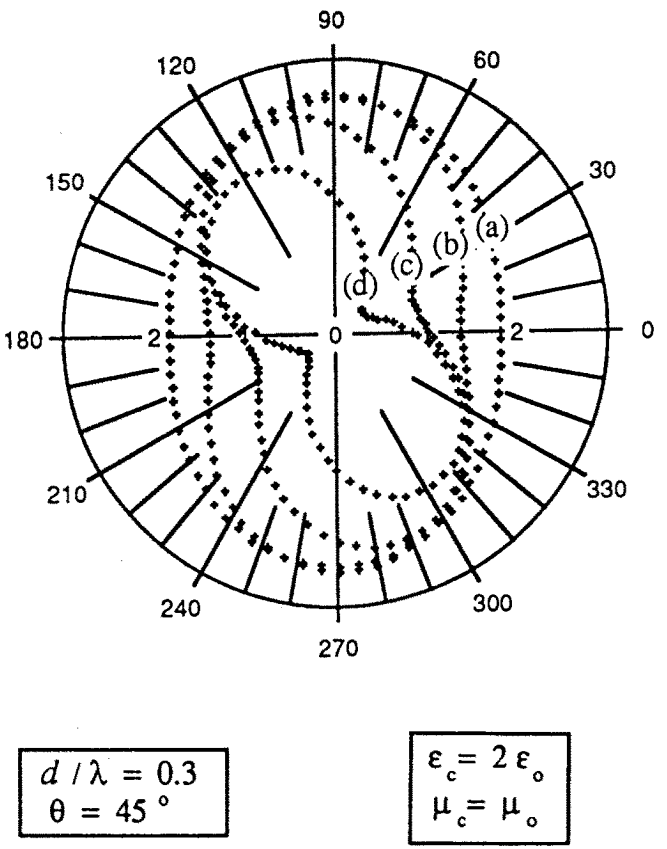

Figure 5. Variation of the radiation pattern of the finite–length thin wire chirostrip antenna of Fig. 1 (placed horizontally along $\varphi = 0,\ 180°$ in the plot) versus azimuthal angle φ for a fixed angle $\theta = 45°$. The normalized slab thickness $d/\lambda_0 = 0.3$, resonant length $L_r (L_r = 0.402\lambda_0$ for $\xi_c = 0$ mho), permittivity $\varepsilon_c = 2\varepsilon_0$, permeability $\mu_c = \mu_0$ and the chirality admittance ξ_c equal to (a) 0 mho, (b) 0.001 mho, (c) 0.0015 mho, and (d) 0.002 mho. This feature is similar to the one analyzed for infinitesimal horizontal chirostrip antenna reported in [22].

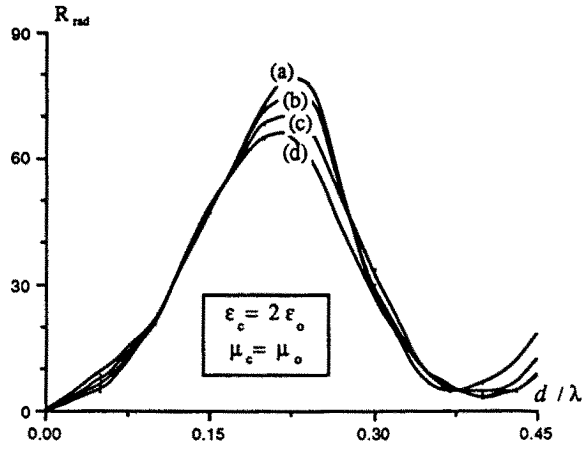

(A)

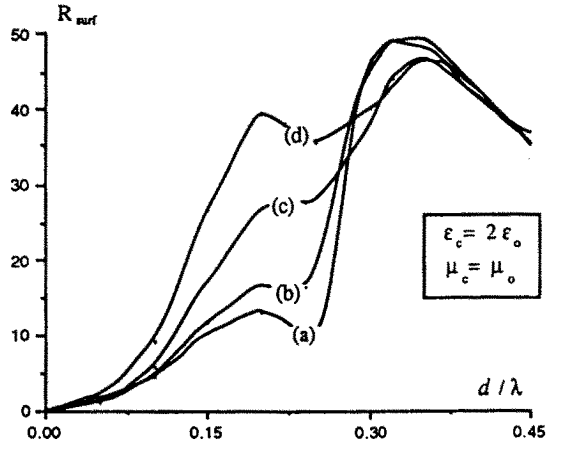

(B)

Figure 6. Radiation resistance of radiated power R_{rad} (shown in (A)) and and of the surface-power R_{surf} (shown in (B)) of the chirostrip antenna of Fig. 1 as a function of the normalized slab thickness d/λ_0 for several values of chirality admittance ξ_c : (a) 0 mho, (b) 0.0005 mho, (c) 0.001 mho, and (d) 0.0015 mho. The radius of the antenna is $a = 0.0001\lambda_0$.

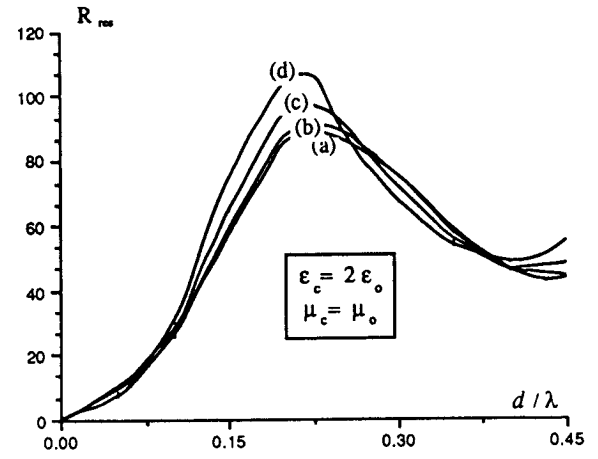

(A)

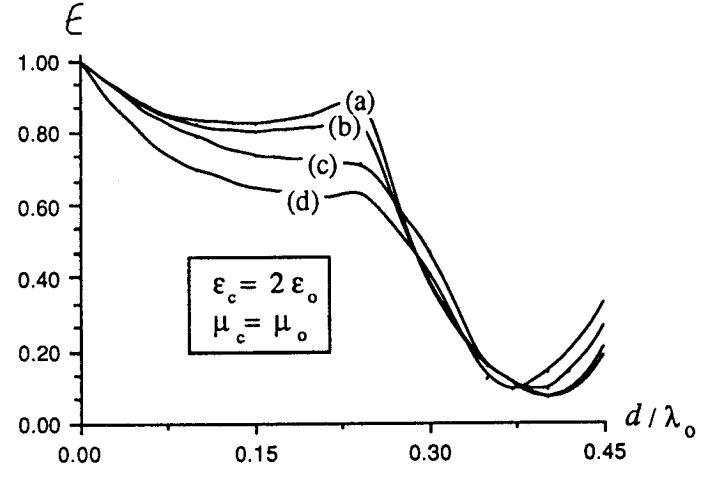

(B)

Figure 7. Total radiation resistance at resonance R_{res} (shown in (A)) and Radiation Efficiency $\in$ (shown in (B)) of the chirostrip antenna of Fig. 1 as a function of the normalized slab thickness d/λ_0 for several values of chirality admittance ξ_c :(a) 0 mho, (b) 0.0005 mho, (c)0.001 mho, and (d) 0.0015 mho. The radius of the antenna is $a = 0.0001\lambda_0$.

are given as functions of the normalized slab thickness d/λ_0 for different values of ξ_c. These plots are given for the resonance case. As can be seen from these figures, adding chirality will increase the total radiation resistance in the resonance. This increase corresponds mostly to an increase in the surface–wave power, a decrease in the radiated power and therefore, and a decrease in the efficiency of the radiating system. However, we must note that although for this antenna the surface–wave power increases with chirality, the angular distribution of such surface waves may vary with chirality leading to modification of mutual coupling between adjacent elements. This mutual coupling has been studied for two finite–length thin–wire chirostrip antennas and the results have been obtained and reported [33]. Furthermore, we have shown that for the two–dimensional infinitely long chirostrip line antenna, the surface–wave power per unit length can, under certain conditions, decrease when the chirality is added to the antenna substrate [20,21]. For a square microstrip patch antenna on a grounded chiral slab, Pozar has also shown a decrease in radiation efficiency due to chirality of substrate [24].

4. Summary

In this paper, we studied theoretically, the radiation characteristics of a particular type of center–fed finite–length thin–wire chirostrip antenna over a thick grounded chiral slab. Using the standard method of moments, we have analyzed and evaluated the current distribution along this antenna when the voltage source at the center gap is a monochromatic source with frequency ω. We have also determined the input impedance of this antenna. In particular, we have investigated the influence of the chirality admittance ξ_c on the current distribution and the input impedance, and have shown that the general form of the current distribution remains almost unchanged when we introduced chirality in the antenna substrate. The input impedance under resonant conditions increases slightly with chirality. The bandwidth and the radiation efficiency of the antenna have also been determined. We have also analyzed the particular rotational feature of the radiation pattern of this finite–length chirostrip antenna and have found results similar to those obtained for the chirostrip horizontal infinitesimal dipole [22]. Like the short dipole case, chirality of the substrate has

caused the radiation pattern to be rotated around the axis perpendicular to the slab by an angle which depends on the chirality admittance ξ_c and the elevation angle. Indeed, the handedness of the slab material has been manifested in the shape of the radiation patterns. Such characteristics may find potential applications in the design of beam–steering systems, or simple radiating devices with complex radiation patterns, since it can involve only a simple finite–length wire antenna. It must also be noted that the chirality may affect the angular distribution of the surface wave excited in the substrate, and although the total surface–wave power can be increased with chirality, the change in surface wave distribution can, under proper conditions, lead to a decrease in mutual coupling between two adjacent elements depending on their relative positions, as studied in [33].

Acknowledgments

Parts of this work were presented at the 1991 North American Radio Science Meeting/International IEEE AP–S Symposium, London, Ontario, Canada, June 24–28, 1991 in the Plenary Session of the URSI Student Prize Paper contest. This work was supported, in part, by the U.S. National Science Foundation under Presidential Young Investigator Grant No. ECS–8957434.

Appendix

In this Appendix, for the sake of easy reference, the expressions of dyadic Green's functions for a grounded chiral slab are given in terms of the cylindrical vector wave functions. The detailed derivation of these expressions can be found in all related bibliographies given in the References e.g., in [23]. Other derivations of dyadic Green's functions for a grounded chiral slab can be found in [18,24–30]. Referring to a geometry similar to Fig. 1, for the case where the current source is located at the point $\mathbf{r}'$ outside the slab, one can divide the dyadic Green's functions into two parts as

Region (1):

$$z \geq d \qquad \overline{\overline{\Gamma}}_c(\mathbf{r},\mathbf{r}') = \overline{\overline{\Gamma}}_c^{11}(\mathbf{r},\mathbf{r}') \tag{1A}$$

Region (2):

$$0 \leq z \leq d \qquad \overline{\overline{\Gamma}}_c(\mathbf{r},\mathbf{r}') = \overline{\overline{\Gamma}}_c^{21}(\mathbf{r},\mathbf{r}') \tag{2A}$$

In (1*A*) and (2*A*), the first superscript indicates the region of the observation point while the second superscript corresponds to the location of the source. These dyadic Green's functions are given as [4]

$$\begin{aligned}\overline{\overline{\Gamma}}_c^{11}(\mathbf{r},\mathbf{r}') = \frac{\mathrm{i}}{4\pi}\int_0^\infty \sum_{n=0}^\infty \frac{d\lambda}{\lambda h_0}(2-\delta_0) \\ \cdot\Big[\Big(a_n^v \overline{\mathbf{V}}_{e_o n\lambda}(h_0) + a_n^w \overline{\mathbf{W}}_{e_o n\lambda}(h_0)\Big)\overline{\mathbf{V}}'_{e_o n\lambda}(h_0) \\ + \Big(b_n^v \overline{\mathbf{V}}_{e_o n\lambda}(h_0) + b_n^w \overline{\mathbf{W}}_{e_o n\lambda}(h_0)\Big)\overline{\mathbf{W}}'_{e_o n\lambda}(h_0) \\ + \begin{cases} \overline{\mathbf{V}}_{e_o n\lambda}(h_0)\overline{\mathbf{V}}'_{e_o n\lambda}(-h_0) + \overline{\mathbf{W}}_{e_o n\lambda}(h_0)\overline{\mathbf{W}}'_{e_o n\lambda}(-h_0) & z \geq z' \\ \overline{\mathbf{V}}_{e_o n\lambda}(-h_0)\overline{\mathbf{V}}'_{e_o n\lambda}(h_0) + \overline{\mathbf{W}}_{e_o n\lambda}(-h_0)\overline{\mathbf{W}}'_{e_o n\lambda}(h_0) & z \geq z' \end{cases}\Big]\end{aligned} \tag{3A}$$

and

$$\begin{aligned}\overline{\overline{\Gamma}}_c^{21}(\mathbf{r},\mathbf{r}') = \frac{\mathrm{i}}{4\pi}\int_0^\infty \sum_{n=0}^\infty \frac{d\lambda}{\lambda h_0}(2-\delta_0) \\ \Big\{c_n^v\Big[\frac{h_-}{k_-}\Big(\overline{\mathbf{V}}_{e_o n\lambda}(h_+) - \overline{\mathbf{W}}_{e_o n\lambda}(-h_+)\Big) \\ + \frac{h_+}{k_+}\Big(\overline{\mathbf{W}}_{e_o n\lambda}(h_-) - \overline{\mathbf{V}}_{e_o n\lambda}(-h_-)\Big)\Big] \\ + c_n^w\Big[\Big(\overline{\mathbf{V}}_{e_o n\lambda}(h_+) + \overline{\mathbf{W}}_{e_o n\lambda}(-h_+)\Big) \\ - \Big(\overline{\mathbf{W}}_{e_o n\lambda}(h_-) + \overline{\mathbf{V}}_{e_o n\lambda}(-h_-)\Big)\Big]\Big\}\overline{\mathbf{V}}'_{e_o n\lambda}(h_0) \\ + \Big\{d_n^v\Big[\frac{h_-}{k_-}\Big(\overline{\mathbf{V}}_{e_o n\lambda}(h_+) - \overline{\mathbf{W}}_{e_o n\lambda}(-h_+)\Big) \\ + \frac{h_+}{k_+}\Big(\overline{\mathbf{W}}_{e_o n\lambda}(h_-) - \overline{\mathbf{V}}_{e_o n\lambda}(-h_-)\Big)\Big] \\ + d_n^w\Big[\Big(\overline{\mathbf{V}}_{e_o n\lambda}(h_+) + \overline{\mathbf{W}}_{e_o n\lambda}(-h_+)\Big)\end{aligned}$$

[4] Since we usually compare the dimensions with free-space wavelength which is shown by λ_0, there should not be any confusion between the variable of integration λ here and the symbol for wavelength λ_0.

$$-\left(\overline{\mathbf{W}}^{e}_{o\,n\lambda}(h_-)+\overline{\mathbf{V}}^{e}_{o\,n\lambda}(-h_-)\right)\Big]\Big\}\,\overline{\mathbf{W}}'^{e}_{o\,n\lambda}(h_0) \tag{4A}$$

where

$$\overline{\mathbf{V}}^{e}_{o\,n\lambda}(h)=\frac{\overline{\mathbf{M}}^{e}_{o\,n\lambda}(h)+\overline{\mathbf{N}}^{e}_{o\,n\lambda}(h)}{\sqrt{2}} \tag{5A}$$

$$\overline{\mathbf{W}}^{e}_{o\,n\lambda}(h)=\frac{\overline{\mathbf{M}}^{e}_{o\,n\lambda}(h)-\overline{\mathbf{N}}^{e}_{o\,n\lambda}(h)}{\sqrt{2}} \tag{6A}$$

with $\mathbf{M}^{e}_{o\,n\lambda}(h)\equiv\nabla\times\overline{\Psi}^{e}_{o\,n\lambda}(h)$ and $\overline{N}^{e}_{o\,n\lambda}(h)\equiv\frac{1}{k}\nabla\times\nabla\times\overline{\Psi}^{e}_{o\,n\lambda}(h)$ for $\overline{\Psi}^{e}_{o\,n\lambda}(h)=J_n(\lambda\rho)\overset{\cos}{\sin}n\varphi\,e^{ihz}\mathbf{e}_z$ in the cylindrical coordinate system (ρ,φ,z). In the above equations, the primed quantities refer to the source point $\mathbf{r}'$ and the unprimed quantities to the observation point $\mathbf{r}$, $\delta_0=1$ if $n=0$, and 0 otherwise, $k^2=\lambda^2+h^2$ where k is the magnitude of the wavenumber in the medium, h is its component along the z-direction and λ is its component along the radial direction. More specifically, $h_0\equiv\sqrt{k_0^2-\lambda^2}$, with $k_0=\omega\sqrt{\mu_0\varepsilon_0}$, $h_\pm\equiv\sqrt{k_\pm^2-\lambda^2}$ and $k_\pm$ have been defined earlier. The coefficients a_n^v, a_n^w, b_n^v, b_n^w, c_n^v, c_n^w, d_n^v, d_n^w are determined by applying boundary conditions for tangential components of electric and magnetic fields $\mathbf{E}$ and $\mathbf{H}$. These coefficients are expressed as

$$[a^v\,;\,a^w\,;\,c^v\,;\,c^w]^T=T^{-1}\left[-e^{-ih_0d}\,;\,\frac{h_0}{k_0}e^{-ih_0d}\,;\,-\frac{k_0}{\mu_0}e^{-ih_0d}\,;\,\frac{h_0}{\mu_0}e^{-ih_0d}\right]^T \tag{7A}$$

$$[b^v\,;\,b^w\,;\,d^v\,;\,d^w]^T=T^{-1}\left[-e^{-ih_0d}\,;\,-\frac{h_0}{k_0}e^{-ih_0d}\,;\,\frac{k_0}{\mu_0}e^{-ih_0d}\,;\,\frac{h_0}{\mu_0}e^{-ih_0d}\right]^T \tag{8A}$$

where

$$T\equiv\begin{pmatrix}T_{11} & T_{12}\\ T_{21} & T_{22}\end{pmatrix}$$

with

$$T_{11}\equiv\begin{pmatrix}e^{ih_0d} & e^{ih_0d}\\ \frac{h_0}{k_0}e^{ih_0d} & -\frac{h_0}{k_0}e^{ih_0d}\end{pmatrix}$$

$$T_{12} \equiv \begin{pmatrix} -2\,\mathrm{i}\left\{\frac{h_-}{k_-}\sin(h_+d) + \frac{h_+}{k_+}\sin(h_-d)\right\} & -2\,\{\cos(h_+d) - \cos(h_-d)\} \\ -2\frac{h_+h_-}{k_+k_-}\{\cos(h_+d) - \cos(h_-d)\} & -2\,\mathrm{i}\left\{\frac{h_+}{k_+}\sin(h_+d) + \frac{h_-}{k_-}\sin(h_-d)\right\} \end{pmatrix}$$

$$T_{21} \equiv \begin{pmatrix} \frac{k_0}{\mu_0}\mathrm{e}^{\mathrm{i}h_0d} & -\frac{k_0}{\mu_0}\mathrm{e}^{\mathrm{i}h_0d} \\ \frac{h_0}{\mu_0}\mathrm{e}^{\mathrm{i}h_0d} & \frac{h_0}{\mu_0}\mathrm{e}^{\mathrm{i}h_0d} \end{pmatrix}$$

$$T_{22} \equiv \frac{k_+ + k_-}{2\mu_c} \begin{pmatrix} -2\,\mathrm{i}\left\{\frac{h_-}{k_-}\sin(h_+d) - \frac{h_+}{k_+}\sin(h_-d)\right\} & -2\,\{\cos(h_+d) + \cos(h_-d)\} \\ -2\frac{h_+h_-}{k_+k_-}\{\cos(h_+d) + \cos(h_-d)\} & -2\,\mathrm{i}\left\{\frac{h_+}{k_+}\sin(h_+d) - \frac{h_-}{k_-}\sin(h_-d)\right\} \end{pmatrix}$$

Here T^{-1} is the inverse of the matrix T, the symbol $[]^T$ denotes the transpose of a matrix. For the case where the electric current source is located at $\mathbf{r}'$ inside the chiral slab, the dyadic Green's functions can be decomposed as

Region (1):

$$z \geq d \qquad \overline{\overline{\Gamma}}_c(\mathbf{r}, \mathbf{r}') = \overline{\overline{\Gamma}}_c^{12}(\mathbf{r}, \mathbf{r}') \tag{9A}$$

Region (2):

$$0 \leq z \leq d \qquad \overline{\overline{\Gamma}}_c(\mathbf{r}, \mathbf{r}') = \overline{\overline{\Gamma}}_c^{22}(\mathbf{r}, \mathbf{r}') \tag{10A}$$

The explicit expressions are

$$
\begin{aligned}
&\overline{\overline{\Gamma}}_c^{12}(\mathbf{r},\mathbf{r}') = \frac{\mathrm{i}}{2\pi(k_+ + k_-)} \\
&\int_0^\infty \sum_{n=0}^{\infty} \frac{d\lambda}{\lambda}(2-\delta_0)\left[\left(a_n^v \overline{\mathbf{V}}_{\substack{e\\o}n\lambda}(h_0) + a_n^w \overline{\mathbf{W}}_{\substack{e\\o}n\lambda}(h_0)\right)\overline{\mathbf{V}}'_{\substack{e\\o}n\lambda}(h_+)\right. \\
&+\left(b_n^v \overline{\mathbf{V}}_{\substack{e\\o}n\lambda}(h_0) + b_n^w \overline{\mathbf{W}}_{\substack{e\\o}n\lambda}(h_0)\right)\overline{\mathbf{W}}'_{\substack{e\\o}n\lambda}(h_-) \\
&+\left(e_n^v \overline{\mathbf{V}}_{\substack{e\\o}n\lambda}(h_0) + e_n^w \overline{\mathbf{W}}_{\substack{e\\o}n\lambda}(h_0)\right)\overline{\mathbf{V}}'_{\substack{e\\o}n\lambda}(-h_+) \\
&\left.+\left(f_n^v \overline{\mathbf{V}}_{\substack{e\\o}n\lambda}(h_0) + f_n^w \overline{\mathbf{W}}_{\substack{e\\o}n\lambda}(h_0)\right)\overline{\mathbf{W}}'_{\substack{e\\o}n\lambda}(-h_-)\right]
\end{aligned}
\tag{11A}
$$

and

$$
\begin{aligned}
&\overline{\overline{\Gamma}}_c^{22}(\mathbf{r},\mathbf{r}') \\
&=\frac{\mathrm{i}}{2\pi(k_+ + k_-)}\int_0^\infty \sum_{n=0}^{\infty}\frac{d\lambda}{\lambda}(2-\delta_0) \\
&\left\{c_n^v\left[\frac{h_-}{k_-}\left(\overline{\mathbf{V}}_{\substack{e\\o}n\lambda}(h_+) - \overline{\mathbf{W}}_{\substack{e\\o}n\lambda}(-h_+)\right)\right.\right. \\
&\left.+\frac{h_+}{k_+}\left(\overline{\mathbf{W}}_{\substack{e\\o}n\lambda}(h_-) - \overline{\mathbf{V}}_{\substack{e\\o}n\lambda}(-h_-)\right)\right] \\
&+c_n^w\left[\left(\overline{\mathbf{V}}_{\substack{e\\o}n\lambda}(h_+) + \overline{\mathbf{W}}_{\substack{e\\o}n\lambda}(-h_+)\right)\right. \\
&\left.\left.-\left(\overline{\mathbf{W}}_{\substack{e\\o}n\lambda}(h_-) + \overline{\mathbf{V}}_{\substack{e\\o}n\lambda}(-h_-)\right)\right]\right\}\overline{\mathbf{V}}'_{\substack{e\\o}n\lambda}(h_+) \\
&+ \\
&\left\{d_n^v\left[\frac{h_-}{k_-}\left(\overline{\mathbf{V}}_{\substack{e\\o}n\lambda}(h_+) - \overline{\mathbf{W}}_{\substack{e\\o}n\lambda}(-h_+)\right)\right.\right. \\
&\left.+\frac{h_+}{k_+}\left(\overline{\mathbf{W}}_{\substack{e\\o}n\lambda}(h_-) - \overline{\mathbf{V}}_{\substack{e\\o}n\lambda}(-h_-)\right)\right] \\
&+d_n^w\left[\left(\overline{\mathbf{V}}_{\substack{e\\o}n\lambda}(h_+) + \overline{\mathbf{W}}_{\substack{e\\o}n\lambda}(-h_+)\right)\right. \\
&\left.\left.-\left(\overline{\mathbf{W}}_{\substack{e\\o}n\lambda}(h_-) + \overline{\mathbf{V}}_{\substack{e\\o}n\lambda}(-h_-)\right)\right]\right\}\overline{\mathbf{W}}'_{\substack{e\\o}n\lambda}(h_-) \\
&+
\end{aligned}
$$

$$
\begin{aligned}
&\Bigg\{ g_n^v \Bigg[\frac{h_-}{k_-} \left(\overline{\mathbf{V}}_{\circ}^{e}{}_{n\lambda}(h_+) - \overline{\mathbf{W}}_{\circ}^{e}{}_{n\lambda}(-h_+) \right) \\
&+ \frac{h_+}{k_+} \left(\overline{\mathbf{W}}_{\circ}^{e}{}_{n\lambda}(h_-) - \overline{\mathbf{V}}_{\circ}^{e}{}_{n\lambda}(-h_-) \right) \Bigg] \\
&+ g_n^w \Bigg[\left(\overline{\mathbf{V}}_{\circ}^{e}{}_{n\lambda}(h_+) + \overline{\mathbf{W}}_{\circ}^{e}{}_{n\lambda}(-h_+) \right) \\
&- \left(\overline{\mathbf{W}}_{\circ}^{e}{}_{n\lambda}(h_-) + \overline{\mathbf{V}}_{\circ}^{e}{}_{n\lambda}(-h_-) \right) \Bigg] \Bigg\} \overline{\mathbf{V}}'_{\circ}{}^{e}{}_{n\lambda}(-h_+) \\
+ \\
&\Bigg\{ h_n^v \Bigg[\frac{h_-}{k_-} \left(\overline{\mathbf{V}}_{\circ}^{e}{}_{n\lambda}(h_+) - \overline{\mathbf{W}}_{\circ}^{e}{}_{n\lambda}(-h_+) \right) \\
&+ \frac{h_+}{k_+} \left(\overline{\mathbf{W}}_{\circ}^{e}{}_{n\lambda}(h_-) - \overline{\mathbf{V}}_{\circ}^{e}{}_{n\lambda}(-h_-) \right) \Bigg] \\
&+ h_n^w \Bigg[\left(\overline{\mathbf{V}}_{\circ}^{e}{}_{n\lambda}(h_+) + \overline{\mathbf{W}}_{\circ}^{e}{}_{n\lambda}(-h_+) \right) \\
&- \left(\overline{\mathbf{W}}_{\circ}^{e}{}_{n\lambda}(h_-) + \overline{\mathbf{V}}_{\circ}^{e}{}_{n\lambda}(-h_-) \right) \Bigg] \Bigg\} \overline{\mathbf{W}}'_{\circ}{}^{e}{}_{n\lambda}(-h_-) \\
+ \\
&\begin{cases}
\dfrac{k_+}{h_+} \overline{\mathbf{V}}_{\circ}^{e}{}_{n\lambda}(h_+) \overline{\mathbf{V}}'_{\circ}{}^{e}{}_{n\lambda}(-h_+) \\
+ \dfrac{k_+}{h_+} \left(\overline{\mathbf{W}}_{\circ}^{e}{}_{n\lambda}(h_+) - \left[\overline{\mathbf{W}}_{\circ}^{e}{}_{n\lambda}(h_-) + \overline{\mathbf{V}}_{\circ}^{e}{}_{n\lambda}(h_-) \right] \right) \overline{\mathbf{V}}'_{\circ}{}^{e}{}_{n\lambda}(h_+) \\
+ \dfrac{k_-}{h_-} \overline{\mathbf{W}}_{\circ}^{e}{}_{n\lambda}(h_-) \overline{\mathbf{W}}'_{\circ}{}^{e}{}_{n\lambda}(-h_-) \\
- \dfrac{k_-}{h_-} \left(\left[\overline{\mathbf{W}}_{\circ}^{e}{}_{n\lambda}(h_+) + \overline{\mathbf{V}}_{\circ}^{e}{}_{n\lambda}(-h_+) \right] - \overline{\mathbf{V}}_{\circ}^{e}{}_{n\lambda}(h_-) \right) \overline{\mathbf{W}}'_{\circ}{}^{e}{}_{n\lambda}(h_-) \\
\qquad\qquad \text{for } z \geq z'
\end{cases} \\
&\begin{cases}
\left[\overline{\mathbf{V}}_{\circ}^{e}{}_{n\lambda}(-h_+) + \overline{\mathbf{W}}_{\circ}^{e}{}_{n\lambda}(h_+) \right] \left[\dfrac{k_+}{h_+} \overline{\mathbf{V}}'_{\circ}{}^{e}{}_{n\lambda}(h_+) - \dfrac{k_-}{h_-} \overline{\mathbf{W}}'_{\circ}{}^{e}{}_{n\lambda}(h_-) \right] \\
- \left[\overline{\mathbf{W}}_{\circ}^{e}{}_{n\lambda}(-h_-) + \overline{\mathbf{V}}_{\circ}^{e}{}_{n\lambda}(h_-) \right] \left[\dfrac{k_+}{h_+} \overline{\mathbf{V}}'_{\circ}{}^{e}{}_{n\lambda}(h_+) - \dfrac{k_-}{h_-} \overline{\mathbf{W}}'_{\circ}{}^{e}{}_{n\lambda}(h_-) \right] \\
\qquad\qquad \text{for } z \leq z'
\end{cases}
\end{aligned}
\tag{12A}
$$

The coefficients a^v, a^w, b^v, b^w, c^v, c^w, d^v, d^w, e^v, e^w, f^v, f^w, g^v, g^w, h^v,

and h^w, where index n has been dropped, are given by

$$[a^v\,;\,a^w\,;\,c^v\,;\,c^w]^T =$$
$$T^{-1}\left[\frac{k_+}{h_+}\left(e^{ih_+d}-2\cos(h_-d)\right);\ \frac{k_+}{h_+}\left(\frac{h_+}{k_+}e^{ih_+d}+2\,i\frac{h_-}{k_-}\sin(h_-d)\right)\right.$$
$$\frac{k_+}{h_+}\frac{k_+ + k_-}{2\mu_0}\left(e^{ih_+d}+2\cos(h_-d)\right)$$
$$\left.\frac{k_+}{h_+}\frac{k_+ + k_-}{2\mu_0}\left(\frac{h_+}{k_+}e^{ih_+d}-2\,i\frac{h_-}{k_-}\sin(h_-d)\right)\right]^T \tag{13A}$$

$$[b^v\,;\,b^w\,;\,d^v\,;\,d^w]^T =$$
$$T^{-1}\left[\frac{k_-}{h_-}\left(e^{ih_-d}-2\cos(h_+d)\right);\ \frac{k_-}{h_-}\left(\frac{h_-}{k_-}e^{ih_-d}+2\,i\frac{h_+}{k_+}\sin(h_+d)\right)\right.$$
$$\frac{k_-}{h_-}\frac{k_+ + k_-}{2\mu_0}\left(-e^{ih_-d}-2\cos(h_+d)\right)$$
$$\left.\frac{k_-}{h_-}\frac{k_+ + k_-}{2\mu_0}\left(\frac{h_-}{k_-}e^{ih_-d}-2\,i\frac{h_+}{k_+}\sin(h_+d)\right)\right]^T \tag{14A}$$

$$[e^v\,;\,e^w\,;\,g^v\,;\,g^w]^T$$
$$=T^{-1}\left[\frac{k_+}{h_+}e^{ih_+d};\ e^{ih_+d};\ \frac{k_+}{h_+}\frac{k_+ + k_-}{2\mu_0}e^{ih_+d};\ \frac{k_+ + k_-}{2\mu_0}e^{ih_+d}\right]^T \tag{15A}$$

$$[f^v\,;\,f^w\,;\,h^v\,;\,h^w]^T =$$
$$=T^{-1}\left[\frac{k_-}{h_-}e^{ih_-d};\ -e^{ih_-d};\ -\frac{k_-}{h_-}\frac{k_+ + k_-}{2\mu_0}e^{ih_-d};\ \frac{k_+ + k_-}{2\mu_0}e^{ih_-d}\right]^T \tag{16A}$$

References

1. Applequist, J.,"Optical activity: Biot's bequest," *Amer. Scient.,* Vol. 75, No. 1, 59–67, Jan.–Feb. 1987.
2. Jaggard, D. L., and N. Engheta, *Chirality in Electrodynamics: Modeling and Applications,* a chapter in Directions in Electromagnetic Wave Modeling, Editors H. L. Bertoni, and L. B. Felsen, Plenum Publishing Corporation, 485–493 , 1991.
3. Lakhtakia, A., V. V. Varadan, and V. K. Varadan, *Time-Harmonic Electromagnetic Fields in Chiral Media,* Springer–Verlag, Berlin, 1989.
4. Lakhtakia, A., (ed.) *Selected Papers on Natural Optical Activity,* SPIE Opt. Eng. Press, Bellingham, WA, 1990.
5. Jaggard, D. L., A. R. Mickelson, and C. H. Papas, "On electromagnetic waves in chiral media," *J. of Appl. Phys.,* Vol. 28, 211–216, 1979.
6. Bassiri, S., N. Engheta and C. H. Papas, "Dyadic green's function and dipole radiation in chiral media," *Alta Frequenza,* LV–2, 83–88, 1986.
7. Kluskens, M. S., and E. H. Newman, "Scattering by a multilayer chiral cylinder," *IEEE Antennas Propogat.,* AP–39, No. 1, 91–96, 1991.
8. Uslenghi, P. L. E., "Scattering by an impedance sphere coated with a chiral layer," *Electromagnetics,* Vol. 10, 201–211, Jan.–Jun. 1990.
9. Jaggard, D. L., N. Engheta and J. Liu, "Chiroshield: a Salisbury/Dallenbach shield alternative," *Electronics Lett.,* Vol. 26, No. 17, 1332–1334, August 16, 1990.
10. Graglia, R. D., P. L. E. Uslenghi, and C. L. Yu, "Electromagnetic oblique scattering by a cylinder coated with chiral layers and anisotropic jump–immittance sheets," *J. Electro. Waves Applic.,* Vol. 6, No. 5/6, 695–720, 1992.
11. Sihvola, A. H., and I. V. Lindell, "Chiral Maxwell–Garnett mixing formula," *Electronics Lett.,*Vol. 26, No. 2,118–119, 1990.
12. Bohren, C. F., "Scattering of electromagnetic waves by an optically active cylinder," *J. Colloid Interface Sci.,* Vol. 66, 105–109, Aug. 1978.
13. Pelet, P., and N. Engheta,"The theory of chirowaveguides," *IEEE Trans. Antennas Propogat.,* Vol. 38, No. 1, 90–98, 1990.

14. Pelet, P., and N. Engheta, "Coupled–mode theory for chirowaveguides," *J. of Appl. Phys.*, Vol. 67, 2742–2745, 1990.
15. Jaggard, D. L., J. C. Liu, A. Grot, and P. Pelet, "Thin wires antennas in chiral media," *Electronics Lett.*, Vol. 27, No. 3, 243–244, 1991. See also Jaggard, D. L., J. C. Liu, A. Grot, and P. Pelet, "Radiation and scattering from thin wires in chiral media," *IEEE Trans. Antennas Propagat.*, Vol. 40, No. 11, 1273–1282, 1992.
16. Bhattacharyya, A. K. G. J. Burke, and E. K. Miller, "Wavenumbers for currents on infinite– and finite–length wires in a chiral medium," *Proceedings of the 1992 IEEE Antennas & Propagation Society International Symposium,* July 18–25, Chicago, AP–S Digest, Vol. 4, 2026–2028, 1992.
17. Engheta, N., "Theory of chirostrip antennas," Abstract in *Proceedings of the 1988 IEEE AP– S/URSI International Symposium,* Syracuse, New York, June 6–10, 1988.
18. Toscano, A., and Vegni, L., "Spectral dyadic green's function formulation for planar integrated structures with a grounded chiral slab," *J. Electro. Waves Applic.*, Vol. 6, No. 5/6, 751–770, 1992.
19. Kluskens, M. S. and E. H. Newman, "A microstrip line on a chiral substrate," *IEEE Trans. Microwave Theory Tech.*, Vol. MTT–39, No. 11, 1889–1891, 1991.
20. Engheta, N., and P. Pelet, "Reduction of surface waves in chirostrip antennas," *Electronics Lett.*, Vol. 27, No. 1, 5–7, January 3, 1991.
21. Pelet, P., and N. Engheta, "Chirostrip antenna: line source problem" *J. Electro. Waves Applic.*, Vol. 6, No. 5/6, 771–794, 1992.
22. Pelet, P., and N. Engheta, "Novel rotational characteristics of radiation patterns of chirostrip dipole antennas" *Microwave and Opt. Tech.Lett.*, Vol. 5, No. 1, 31–34, January 1992.
23. Pelet, P., "Chirality in guided–wave structures and printed–circuit antennas: theory and applications," PhD Dissertation, Department of Electrical Engineering, University of Pennsylvania, May 1991.
24. Pozar, D., "Microstrip antennas and arrays on chiral substrates," *IEEE Trans. Antennas Propagat.*, Vol. AP–40, No. 10, 1260–1263, 1992.

25. Bhattacharyya, A. K. and A. Lakhtakia, "Initial work on microstrip antenna with chiral substrate: Beltrami field formulation in a generalized cylindrical system," *Archiv für Elektronik und Übertragungstechnik,* Vol. 47, No. 1, 43–45, 1993.
26. Yin, W., and W. Wang, "The dyadic Green's function for the cylindrical chirostrip antenna," *Internat. J. of Infrared and Millimeter Waves,* Vol. 14, No. 4, 849–862, 1993.
27. Yin, W., and W. Wang, "Dyadic Green's function of cylindrical multilayered chiral media and its applications," *J. Electro. Waves and Applic.,* Vol. 7, No. 7, 1005–1027, 1993.
28. Yin, W., and W. Wang, "Analyzing the radiated characteristics of a two–layered chirostrip dipole antenna using the dyadic Green's function," *Microwave and Opt. Tech. Lett,* Vol. 6, No. 4, 221–223, 1993.
29. Ren, W., "Dyadic Green's functions and dipole radiations in layered chiral media," *J. of Appl. Phys.,* Vol. 75, No. 1, 1–6, 1994.
30. Ali, S. M., T. M. Habashy and J. A. Kong, "Spectral–domain dyadic Green's function in layered chiral media," *J. Opt. Soc. Am.,* A9, 413–423, 1992.
31. Nakano, H., S. R. Kerner, and N. G. Alexopoulos, "The moment method solution for printed wire antennas of arbitrary configurations," *IEEE Trans. Antennas Propogat.,* Vol. 36, No. 12, 1667–1673, 1988.
32. Katehi, P. B., and N. G. Alexopoulos, "On the effect of substrate thickness and permittivity on printed–circuit dipole properties," *IEEE Trans. Antennas Propagat.,* Vol. AP–31, No. 1, Jan. 1983.
33. Pelet, P., and N. Engheta, "Mutual coupling in finite–length thin wire chirostrip antennas," *Microwave and Opt. Tech. Lett.,* Vol. 6, No. 9, 671–675, September 1993.